Accurate Automatic Localization of Surfaces of Revolution for Self-Calibration and Metric Reconstruction

Carlo Colombo Dario Comanducci Alberto Del Bimbo Federico Pernici

Abstract— **In this paper, we address the problem of the automatic metric reconstruction Surface of Revolution (SOR) from a single uncalibrated view. The apparent contour and the visible portions of the imaged SOR cross sections are extracted and classified. The harmonic homology that models the image projection of the SOR is also estimated. The special care devoted to accuracy and robustness with respect to outliers makes the approach suitable for automatic camera calibration and metric reconstruction from single uncalibrated views of a SOR. Robustness and accuracy are obtained by embedding a graph-based grouping strategy (Euclidean Minimum Spanning Tree) into an Iterative Closest Point framework for projective curve alignment at multiple scales. Classification of SOR curves is achieved through a 2-dof voting scheme based on a pencil of conics novel parametrization. The main contribution of this work is to extend the domain of automatic single view reconstruction from piecewise planar scenes to scenes including curved surfaces, thus allowing to create automatically realistic image models of man-made objects. Experimental results with real images taken from the internet are reported, and the effectiveness and limitations of the approach are discussed.**

I. Introduction and Related Work

The confluence of projective geometry and computer vision has produced recently impressive results in image based modeling. In particular, self-calibration methods have been developed to support metric 3D reconstruction even from single uncalibrated views. However, single view reconstruction is typically performed in a semi-automatic way, due to the difficulties arising in automatic image segmentation [1] [2] [3]. Automatic segmentation for reconstruction is even more challenging than for recognition, since accurate estimates of geometric features and their relationships are needed in order to get reasonable calibration results. The use of geometric models of the scene can ease the automatic segmentation task, by reducing the hypothesis search space during the process. In [4] [5] [6] [7], a piecewise planar scene model was used to support segmentation for reconstruction.

Models of non planar surfaces such as the Straight Homogeneous Generalized Cylinder (SHGC) were extensively used in the past for the specific problem of segmentation for recognition under affine view conditions (for a review, see [8]). Recent work on this problem is described in [9], where a bottom-up strategy is used to recognize SHGC models from B-spline interpolated image curves. Similar time consuming bottom-up strategies are also exploited in other approaches performing curve segmentation without a specific 3D model [10] [11] [12].

The most recent research in the domain of single view camera calibration and reconstruction has focused on Surfaces Of Revolution (SOR's), which are a subclass of SHGC's. In [13] it is shown that a single SOR view can provide two constraints to partially calibrate a pinhole camera. Semi-automatic approaches extending single view planar scene reconstruction to the SOR case were presented in [14] and [15]. In particular, the latter approach also shows how to perform texture acquisition from a single SOR view.

In this paper, a method for the automatic segmentation of SOR models from a single uncalibrated perspective view is presented. The method is aimed at supporting single view reconstruction, and make it fully automatic. A top-down segmentation strategy is devised, in which a global projective model and the image curves consistent with it are estimated at multiple scales. The estimation interleaves robust curve alignment and graph-based curve grouping. The segmented image curves are then classified into apparent contour and imaged SOR cross sections by means of a voting scheme based on the projective properties of imaged SOR's. The paper is organized as follows. In the following section, the segmentation problem is stated, and an outline of its solution is provided. In Sect. III, model estimation and curve grouping is described. Curve classification is addressed in Sect. IV. In Sect. V experimental results are discussed; finally, conclusions and directions for further research are presented in Sect. VI.

II. Problem Statement and Overview of the Approach

The perspective projection of a SOR like the bell of Fig. 1(a) gives rise to two different kinds of image curves, namely the *apparent contour* and the *imaged cross sections*. The apparent contour is the image of the points at which the surface is smooth and the projection rays are tangent to the surface. The shape of this curve is view dependent. On the other hand, imaged cross sections are view independent elliptical curves, which correspond to parallel coaxial circles in 3D and arise from surface normal discontinuities or surface texture content. Both the apparent contour and the imaged cross sections of a SOR are transformed onto themselves by a 4-dof harmonic homology

$$\mathtt{H} = \mathtt{I} - 2\frac{\mathbf{v}_\infty \mathbf{l}_s^{\mathrm{T}}}{\mathbf{v}_\infty^{\mathrm{T}} \mathbf{l}_s} \ , \tag{1}$$

where $\mathbf{v}_\infty$ and $\mathbf{l}_s$ are respectively the vanishing point and the imaged axis of revolution of the normal direction of the plane

(a)

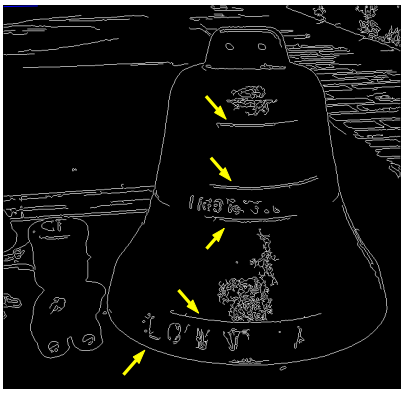

(b)

Fig. 1. (a): original SOR image. (b): the edge image of (a), several cross-section fragments are visible (indicated with arrows); yet, these measurements are practically useless for classic ellipse detection and estimation algorithms.

passing through $\mathbf{l}_s$ and the camera center [16].

The problem addressed here is how to estimate automatically from a SOR image the harmonic homology of Eq. 1 together with the apparent contour and the visible imaged cross sections consistent with it. This geometric information is useful to perform both camera calibration and metric reconstruction of a SOR object based on a single uncalibrated view. This problem could hardly be solved without embedding the full geometric knowledge of the scene into the estimation process. For instance, as shown in Fig. 1(b), the visible segments of the imaged cross sections typically correspond to almost straight edgel chains, thus making their extraction highly inaccurate or even impossible with standard ellipse detectors. The approach followed in this work, sketched hereafter, attempts to exploit as much as possible the prior knowledge of the scene in order to tightly constrain the estimation process.

The overall approach can be divided into two phases: (1) estimation of the harmonic homology of Eq. 1 and of all image curves consistent with it (see Sect. III); (2) classification of the image curves (see Sect. IV). The first phase uses an Iterative Closest Point (ICP) strategy [17][18] to align sets of edgels related by the harmonic homology as the result of a nonlinear optimation problem. (Edgels are obtained by Canny edge detection.) The main advantage of using ICP is that it allows to represent curves globally as noisy point sets, thus avoiding any intermediate representation by local descriptors, which are typically cumbersome to extract and unreliable. In order to cope with a large fraction of outliers – i.e., edgels not belonging to the SOR –, the approach makes an extensive use of robust regression methods, such as the Least Median of Squares (LMedS) [19]. Outlier rejection also benefits from the use of a general curve grouping scheme based on continuity properties. Moreover, in order to avoid to get stuck in local minima during the nonlinear minimization, ICP is run at multiple scales and applied to subsequent levels of a Gaussian pyramid. ICP algorithms generally need an initial alignment in order to converge. At the beginning of the first phase, the RANdom SAmple Consensus (RANSAC) algorithm is run at the coarsest pyramid level so as to provide ICP with a reliable first guess solution. The second phase is devoted to classifying the image curves obtained in the first phase respectively into (a) apparent contour, (b) imaged cross sections and (c) clutter. To this end, ellipses are searched for over the image as particular instances of a conic pencils spanning the apparent contour.

III. Homology Estimation and Curve Grouping

a) **RANSAC-based initialization.:** To compute a weak estimate of the harmonic homology and use it as a first guess for the whole estimation process, bitangents to imaged SOR curves could be used as shown in [20] [13]. However, bitangent estimation generally requires that the Canny edgels be interpolated by polynomials. To avoid this heavy computational step, an alternative way is to estimate the homology directly from the edgels. This is achieved by running RANSAC at the coarsest level of the pyramid. RANSAC is a random sampling procedure which is known to be slow in the presence of a large number of outliers and/or model parameters. In fact, the number N of RANSAC trials which guarantees the statistical convergence depends on the percentage of outlier to tolerate: $N = \frac{\log(1-p)}{\log(1-(1-\epsilon)^s)}$, where ϵ is the fraction of outliers present in the data and s is the number of points of the sample set (p is a probability value generally set to 0.99). If the sample set and the outlier percentage are low, a fast convergence is obtained. This is what happens at the coarsest level of the pyramid, since (*i*) due to low pass filtering, the number of edgels – and therefore, of possible outliers – is small; (*ii*) the harmonic homology reduces to Euclidean axial symmetry, which can be described by the 2-dof axis $\mathbf{l}_s$ only – the vanishing point $\mathbf{v}_\infty$ being the point at infinity in the direction orthogonal to the axis. Fig. 2(a) shows the estimated axial symmetry for the bell of Fig. 1.

b) **Robust homology estimation.:** At each level of the pyramid, the harmonic homology is estimated starting from the results obtained at the immediately coarser level by directly minimizing the registration error

$$\mathcal{F}(\mathbf{l}_s, \mathbf{v}_\infty) = \sum_i \|\mathbf{x}'_i - \mathtt{H}(\mathbf{l}_s, \mathbf{v}_\infty)\mathbf{x}_i\|^2 + \sum_i \|\mathbf{x}_i - \mathtt{H}^{-1}(\mathbf{l}_s, \mathbf{v}_\infty)\mathbf{x}'_i\|^2 \quad (2)$$

using nonlinear optimization. In Eq. 3, $\mathbf{x}_i$ and $\mathbf{x}'_i$ are edgel points corresponding under $\mathtt{H}$. In particular, since $\mathtt{H}^{-1} = \mathtt{H}$, $\mathcal{F}$ is a symmetric transfer error – a distance measure with a remarkable geometric meaning. To reject outliers and also to improve convergence, the LMedS is used. Its effect is to reduce, by selecting them, the points involved in Eq. 3. Once the histogram of symmetric transfer distances is computed, only the points inside six times the standard deviation from the mode are retained.

Figs. 2(b) and 2(c) show the estimation results obtained at the first and second pyramid levels, respectively. In particular, the result of Fig. 2(b) is an improvement of the RANSAC result shown in Fig. 2(a), and represents the initial guess for the result of Fig. 2(c). Note that although new edgels arise at each finer resolution level, the homology estimate (whose axis is shown in the figures) remains locked to the dominant SOR.

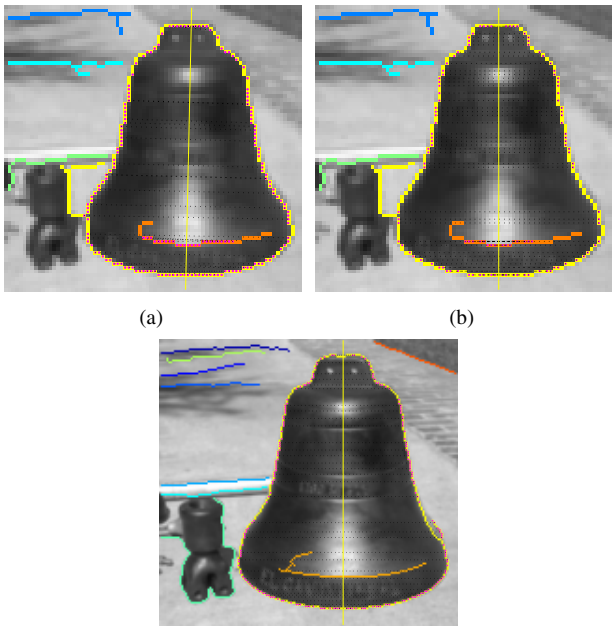

(a) (b) (c)

Fig. 2. ICP homology RANSAC initialization (a) and estimation at the end of the 1st (b) and 2nd (c) levels of the pyramid. Each level uses as initial guess the results of the previous one.

c) **Curve Grouping.:** Despite the fact that the multiresolution approach together with LMedS heavily contributes to regularize the error surface, the non linear minimization strategy above can get stuck in local minima in the presence of a huge number of outliers. This is typically the case when the background clutter and/or the SOR texture accidentally exhibit symmetric patterns which act as distractors. In order to cope with this situation, further prior knowledge about the geometric characteristics of imaged SOR curves is exploited. Indeed, only those image curves which (1) are long and dense, and (2) have tangents which also correspond under the homology should contribute to the minimization. To check the above criteria, curves have to be constructed from edgels. An efficient way to do this is to compute the Euclidean Minimum Spanning Tree (EMST) for the whole set of edgels. This is obtained by running the Kruskal algorithm on the Delaunay triangulation graph computed over the whole edgel set [21]. The assumption that the edgels lie on regular curves allows for the removal of inconsistent arcs from the EMST, whose remaining connected components are the required image curves. Arc removal is achieved by performing simple topological testing. Indeed, since each curve is regular, multiple branching from an edgel is not allowed. Therefore, all arcs but two at any branching point of the EMST must be removed. In particular, to meet the denseness requirement, the longest arcs are removed. The gradient direction information associated to each edgel is also exploited to check the local tangency requirement. In particular, given the point transformation $\mathtt{H}$, tangent lines must correspond under $\mathtt{H}^{-\mathrm{T}}$. Edgels whose tangent lines do not correspond are not put into correspondence in the ICP procedure. Fig. 3(a) shows the EMST for the last level of the pyramid (bell image). Fig. 3(b) shows the result of arc removal at branching points. Fig. 3(c) shows the remaining connected components, i.e. the resulting image curves. The figures show the results for one of the two half planes generated by $\mathbf{l}_s$. Indeed, due to symmetry under the homology, the edgel set belonging to any half plane is sufficient for curve grouping purposes.

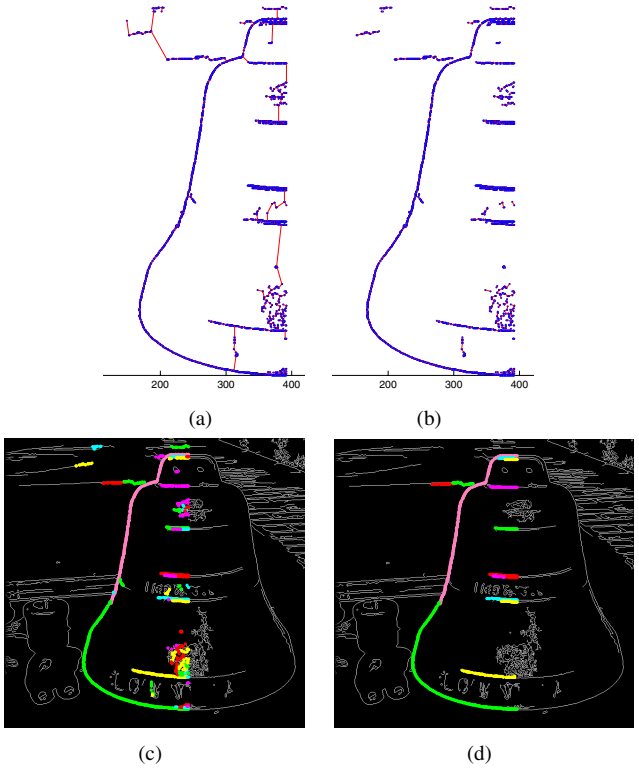

(a) (b) (c) (d)

Fig. 3. (a): the EMST of the original image (finer pyramid level). (b): arc removal from branching points. (c): the curves resulting from arc removal. (d): the curves resulting after saliency thresholding.

After arc removal, the obtained image curves $\mathcal{C}_k, k =$

$1, \dots K$ are scored by means of the following saliency measure:

$$S(\mathcal{C}_k) = \frac{M}{\frac{1}{M-1}\sum_{j=1}^{M-1} d(\mathbf{x}_i, \mathbf{x}_{i+1})} \ , \qquad (3)$$

where M is the number of edgels of the curve and $d(\mathbf{x}_i, \mathbf{x}_{i+1})$ is the Euclidean distance between subsequent edgels. This measure assigns high scores to dense, long curves and low scores to short, fragmented ones. This allows for using LMedS again to keep only the curves which lie outside the mode. Fig. 3(d) shows the curves of Fig. 3(c) after saliency thresholding.

d) **Summary.:** The homology estimation and curve grouping algorithm is summarized as:

0. Compute the Gaussian pyramid $\{G_l\}, l = 0 \dots L-1$ and extract the edgels at all levels.
1. Set $l = 0$ (coarsest level). Compute $\mathtt{H}^{(l)}$ from the edgels of G_0 with RANSAC.
2. Repeat until convergence:
   - Transform each edgel $\mathbf{x}_i$ with $\mathtt{H}^{(l)}$ and compute the edgel closest to $\mathtt{H}^{(l)}\mathbf{x}_i$.
   - Discard all edgel pairs whose tangent lines do not correspond under $[\mathtt{H}^{(l)}]^{-\mathrm{T}}$.
   - Compute the inlier set $\{\mathbf{x}_i\}$ from the histogram of distances with LMedS.
   - Compute the EMST from the points of $\{\mathbf{x}_i\}$.
   - Remove all but two arcs from the EMST branching points and obtain the set of curves $\{\mathcal{C}_k\}$.
   - Compute the histogram of the saliency and the inliers from $\{\mathcal{C}_k\}$ with LMedS.
   - Update the homology as $\mathtt{H}^{(l)} \leftarrow \arg\min_{\mathtt{H}^{(l)}} \mathcal{F}(\mathbf{l}_s, \mathbf{v}_\infty)$ by nonlinear optimization.
3. If $l < L$, set $l \leftarrow l+1$ and go to 2.

IV. Curve Classification

In this section a novel method is presented to classify curves extracted from a SOR image into three classes: apparent contour, imaged cross section (ellipse), clutter. The third class includes all the curves that are not part of the dominant SOR object in the scene. The classification strategy is based on the following result (see also Fig. 4):

Given two curves γ and γ' and two points on them, $\mathbf{x} \in \gamma$ and $\mathbf{x}' \in \gamma'$, which correspond under H*, then all the possible imaged SOR cross sections through $\mathbf{x}$ and $\mathbf{x}'$ are described by the 1-dof pencil of conics*

$$\mathtt{C}(\lambda) = \mathbf{m}\mathbf{m}^{\mathrm{T}} + \lambda(\mathbf{l}\mathbf{l}'^{\mathrm{T}} + \mathbf{l}'\mathbf{l}^{\mathrm{T}}) \ , \qquad (4)$$

where $\mathbf{m}\mathbf{m}^{\mathrm{T}}$ is the (rank 1) degenerate conic composed by the line $\mathbf{m} = \mathbf{x}' \times \mathbf{x}$ through $\mathbf{x}'$ and $\mathbf{x}$, and $\mathbf{l}\mathbf{l}'^{\mathrm{T}} + \mathbf{l}'\mathbf{l}^{\mathrm{T}}$ is the (rank 2) degenerate conic composed by the line pair $\mathbf{l}$ and $\mathbf{l}'$ tangent to γ and γ' (the two symmetric side of the apparent contour) respectively at $\mathbf{x}$ and $\mathbf{x}'$.

To prove this result, it is sufficient to recall that the apparent contour is tangent to an imaged SOR cross section at any point of contact [8]. This means that, at the point of contact, the apparent contour and the ellipse have the same tangent line. Fig. 4 shows two symmetric portions γ and γ' of the apparent contour, corresponding under the harmonic homology

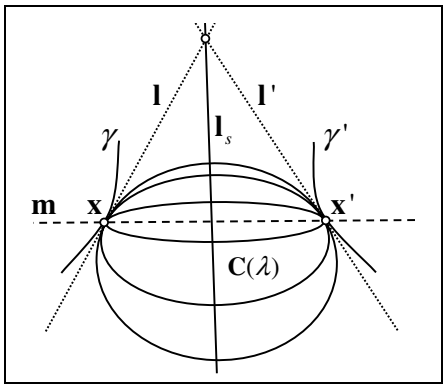

Fig. 4. The pencil of conics at the tangent contact points $\mathbf{x}$ and $\mathbf{x}'$ of the apparent contour of a SOR. Three members of the pencil are reported for three distinct values of λ.

with axis $\mathbf{l}_s$. If the tangent lines $\mathbf{x} \in \gamma$ and $\mathbf{x}' \in \gamma'$ are $\mathbf{l}$ and $\mathbf{l}'$ respectively, then all the possible imaged cross sections $\mathtt{C}$ must include $\mathbf{x}$ and $\mathbf{x}'$ and have there as tangent lines $\mathbf{l}$ and $\mathbf{l}'$ respectively. From the point inclusion constraints $\mathbf{x}^{\mathrm{T}}\mathtt{C}\mathbf{x} = 0$ and $\mathbf{x}'^{\mathrm{T}}\mathtt{C}\mathbf{x}' = 0$ and the tangency constraints $\mathtt{C}\mathbf{x}' \times \mathbf{l}' = \mathbf{0}$ and $\mathtt{C}\mathbf{x} \times \mathbf{l} = \mathbf{0}$ the result follows immediately.

It is also straightforward to show that there exists a closed form solution for the member of the pencil passing through any assigned point $\mathbf{p}$, i.e. such that $\mathbf{p}^{\mathrm{T}}\mathtt{C}(\lambda_{\mathtt{p}})\mathbf{p} = 0$:

$$\lambda_{\mathtt{p}} = -\frac{\mathbf{p}^{\mathrm{T}}(\mathbf{m}\mathbf{m}^{\mathrm{T}})\mathbf{p}}{\mathbf{p}^{\mathrm{T}}(\mathbf{l}\mathbf{l}'^{\mathrm{T}} + \mathbf{l}'\mathbf{l}^{\mathrm{T}})\mathbf{p}} \ . \qquad (5)$$

This last result can be used to formulate the curve classification algorithm as a voting procedure similar to the Hough transform. The algorithm is as follows.

0. Repeat steps 1–3 for all the ordered pairs ($\mathcal{C}_i$,$\mathcal{C}_j$).
1. Consider $\mathcal{C}_i$ from the curve set $\{\mathcal{C}_k\}$, assume that it belongs to the apparent contour, and parametrize it as $\mathbf{x}_m$, with m an integer spanning all the edgels of $\mathcal{C}_i$. For each value of m, a pencil $\mathtt{C}_m(\lambda)$ is obtained.
2. Consider a second curve $\mathcal{C}_j$, and parametrize it as $\mathbf{x}_n$. For all values of n, use Eq. 5 to find the value λ_n such that $\mathbf{x}_n^{\mathrm{T}}\mathtt{C}_m(\lambda_n)\mathbf{x}_n = 0$.
3. Let $v(m,n)$ be the fraction of points of $\mathcal{C}_j$ whose distance from $\mathtt{C}_m(\lambda_n)$ is below a predefined threshold δ (we use 1 pixel). If the peak value $v(m^\star, n^\star)$ of the matrix $\{v(m,n), \ \forall m \forall n\}$ is above 0.9, then classify $\mathcal{C}_i$ as a portion of the apparent contour, and $\mathcal{C}_j$ as a portion of the imaged cross section $\mathtt{C}_{m^\star}(\lambda_{n^\star})$.

V. Experimental Results

In order to test the algorithm for SOR detection and homology estimation discussed in Sect. III, a set of 37 SOR images was considered. In order to have a ground truth for experiments, for each image of the set the dominant SOR was identified, and the associated harmonic homology was computed from hand drawn apparent contours. The dominant SOR was correctly detected with the proposed algorithm in the 93% of the cases. Moreover, the average departure of

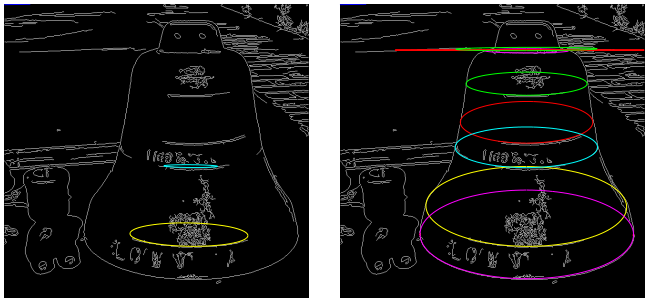

(a) (b)

Fig. 5. (a): Two ellipses fitted with the algorithm described in [22]. (b): The results of the proposed ellipse classification algorithm.

the harmonic homology axis computed automatically from the ground truth axis is 0.6 degrees. The main source of error for the SOR detection algorithm is the presence of planar scene structures exhibiting a high degree of symmetry, giving rise to harmonic homologies which do not actually correspond to a SOR.

Concerning curve classification, results show that the algorithm of Sect. IV is always correct in finding the SOR apparent contour, and also provides ellipse estimates which are far more reliable than the ones obtained with classical ellipse estimation algorithms. Fig. 5 shows the results of ellipse estimation obtained respectively with the algorithm described in [22] on two manually selected curves (Fig. 5(a)), and with the algorithm proposed in this paper (Fig. 5(b)).

Curve classification takes about two minutes per image on a 1.5Ghz computer. Generally, most of the computation is spent on the last pyramid level (the original image), where a huge number of edgels is extracted. Timings are measured with images of medium size (640×480 or 800×600) and 4 or 5 pyramid levels.

The algorithms proposed here were used to support the method for camera calibration and metric reconstruction from single uncalibrated SOR images described in [15]. All images were taken from the internet. Results are shown in Figs. 6, 7 and 8. Fig. 6(a) and 6(b) show the effectiveness of results for the metric reconstruction of the bell of Fig. 1. Estimation results are good enough to calibrate the camera and perform both metric reconstruction and texture acquisition as described in [15]. Fig. 6(c) shows the acquired texture, in which imaged cross sections and SOR meridians become orthogonal straight lines. Fig. 6(d) shows the image rectification of the plane the bell is laid. The detected ellipses furnish also the homography which reports to metric the planar geometry of the SOR ground plane. An example with a vase image is also presented. Fig. 7(c) shows the original image with the superimposed interpolated curves. Figs. 7(a) and (b) show the non interpolated curves before and after saliency thresholding. Finally, Fig. 7(d) reports the reconstructed 3D model. Fig. 8(a) is an image showing the Taj Mahal. Fig. 8(b) shows a synthetic view of the reconstructed dome of the Taj Mahal.

The algorithm may fail when the shadows is present nearly

(a) (b)

(c) (d)

Fig. 6. Applications. (a),(b): two synthetic views of the reconstructed bell of Fig. 1. (c): metric flattened texture of the bell surface (the imaged cross-section looks straight). (d): metric rectification of the floor inferred from the SOR.

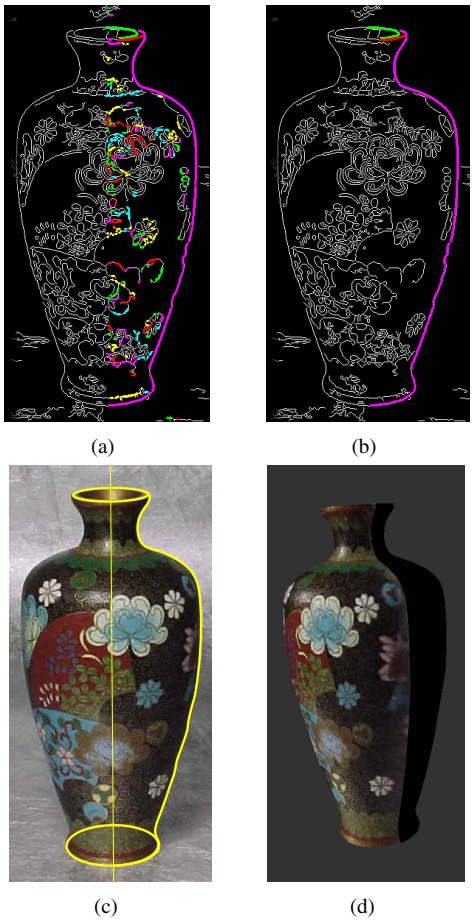

(a) (b)

(c) (d)

Fig. 7. (a), (b): Curve grouping before and after saliency thresholding for the vase shown in (c). (c): the original vase with superimposed the spline curve and the ellipses used for metric reconstruction. (d): A view for the reconstructed vase.

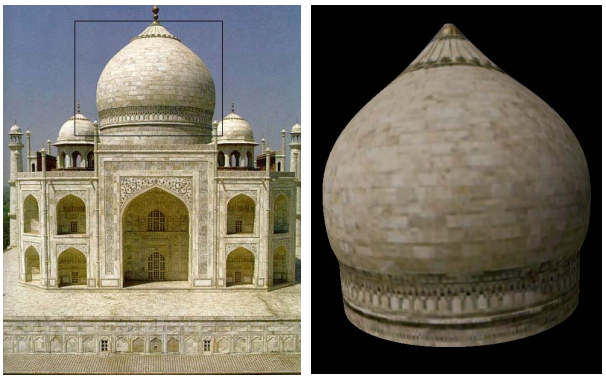

(a) (b)

Fig. 8. (a): The Taj Mahal. (b): The reconstructed dome.

the apparent contour as shown in Fig.9(a). This problem arise since the detected edges of the two curves (the apparent contour and the shadow boundary) are very close to each other. This produce a slightly deviating symmetry which can be erroneously detected by the RANSAC initialization as shown in Fig.9(b). This also prevent the convergence of the nonlinear minimization to a global minimum (Fig.9(c)).

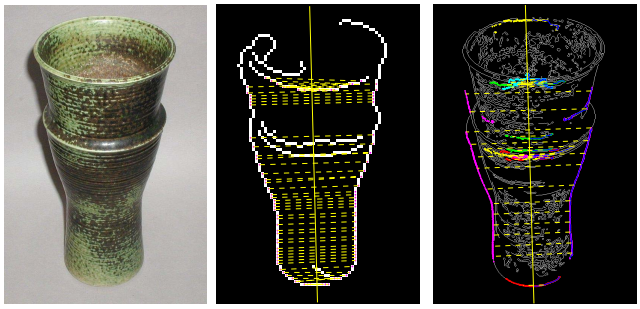

(a) (b) (c)

Fig. 9. (a): A SOR view in which the algorithm may fail. (b): The RANSAC initialization at the coarsest level. The shadow boundary edges are erroneously classified as symmetric. The dotted lines indicates corresponding points. (c): The final result. The nonlinear minimization remain trapped in a local minima.

VI. Conclusion and Future Work

An original approach to automatically grouping and estimation of the projective geometry of single SOR views was presented. The approach is mainly devoted to camera autocalibration from a single SOR view and single view metric reconstruction of SOR objects.

The main limitation of the approach is related to the possibility of misdetections due to symmetric line patterns acting as distractors. To overcome this limitation, further research will be devoted to combining in a single general framework the SOR and planar cases. Another limitation is that curve differentiability is required in order to use Eq. 4 for the purpose of ellipse detection. This requirement prevents from estimating all ellipses corresponding to surface normal discontinuities.

References

[1] P. Sturm and S. Maybank, "A method for interactive 3d reconstruction of piecewise planar objects from single images," in *British Machine Vision Conference, Nottingham, England*, Sep 1999, pp. 265–274.

[2] H.-Y. Shum, R. Szeliski, S. Baker, M. Han, and P. Anandan, "Interactive 3d modeling from multiple images using scene regularities," in *Proceedings of the European Workshop on 3D Structure from Multiple Images of Large-scale Environments (at ECCV '98)*, 1998.

[3] D. Liebowitz, A. Criminisi, and A. Zisserman, "Creating architectural models from images," in *Proc. EuroGraphics*, vol. 18, September 1999, pp. 39–50.

[4] F. Schaffalitzky and A. Zisserman, "Planar grouping for automatic detection of vanishing lines and points," vol. 18, pp. 647–658, 2000.

[5] A. Bartoli., "Piecewise planar segmentation for automatic scene modeling," *CVPR'01 - In Proceedings of the IEEE International Conference on Computer Vision and Pattern Recognition*, vol. vol. II, pp. 283–289, December 2001.

[6] C. Baillard and A. Zisserman, "Automatic reconstruction of piecewise planar models from multiple views," in *Proceedings of the IEEE Conference on Computer Vision and Pattern Recognition*, jun 1999, pp. 559–565.

[7] A. Dick, P. Torr, S. Ruffle, and R. Cipolla, "Combining single view recognition and multiple view stereo for architectural scenes," *In Proceedings of the 8th International Conference on Computer Vision, Vancouver, Canada*, 2001.

[8] S. M. Abdallah, "Object recognition via invariance," Ph.D. dissertation, The University of Sydney, Australia, June 2000.

[9] M. Zerroug and R. Nevatia, "Volumetric descriptions from a single intensity image." *International Journal of Computer Vision*, vol. 20(1/2), pp. 11–42, 1996.

[10] P. Rosin and G. West., "Non-parametric segmentation of curves into various representations." *PAMI*, vol. 17, no. 12, pp. 1140–1153, December 1995.

[11] D. S. Chen, "A data-driven intermediate level feature extraction algorithm," *IEEE Transactions On Pattern Analysis And Machine Intelligence*, vol. 11, no. 7, pp. 749–758, 1989.

[12] R. F. M. Pilu, "Model-driven grouping and recognition of generic object parts from single images," *Proc. 4th Int. Symp. on Intelligent Robotic Systems, Lisbon*, pp. 147–154, July 1996.

[13] K.-Y. K. Wong, P. R. S. Mendonça, and R. Cipolla, "Camera calibration from surfaces of revolution," *PAMI*, vol. 25, no. 2, pp. 147–161, February 2003.

[14] ——, "Reconstruction of surfaces of revolution from single uncalibrated views," in *Proc. British Machine Vision Conference 2002*, P. L. Rosin and D. Marshall, Eds., vol. 1. Cardiff, UK: British Machine Vision Association, September 2002, pp. 93–102.

[15] C. Colombo, A. DelBimbo, and F. Pernici, "Uncalibrated 3D metric reconstruction and flattened texture acquisition from a single view of a surface of revolution," *3DPVT02*, pp. 277–284, 2002.

[16] J. Mundy and A. Zisserman, "Repeated structures: Image correspondence constraints and ambiguity of 3D reconstruction," in *Applications of invariance in computer vision*, J. Mundy, A. Zisserman, and D. Forsyth, Eds. Springer-Verlag, 1994, pp. 89–106.

[17] N. M. P.J. Besl, "A method for registration of 3-d shapes," *IEEE Trans. on Pattern Analisys and Machine Intelligence*, vol. 14, no. 2, pp. 239–256, 1992.

[18] R. Fisher, "Projective icp and stabilizing architectural augmented reality overlays," *Proc. Int. Symp. on Virtual and Augmented Architecture (VAA01), Dublin, Ireland,*, pp. 69–80, Jun 2001.

[19] A. M. L. Peter J. Rousseeuw, *Robust Regression and Outlier Detection*. ISBN: 0-471-85233-3: John Wiley and Sons, December 1987.

[20] D. A. Forsyth, J. L. Mundy, A. Zisserman, and C. A. Rothwell, "Recognising rotationally symmetric surfaces from their outlines," in *Proc. European Conference on Computer Vision*, ser. LNCS 588. Springer-Verlag, 1992.

[21] L. H. de Figueiredo and J. Gomes, "Computational morphology of curves," *The Visual Computer*, vol. 11, no. 2, pp. 105–112, 1995.

[22] A. W. Fitzgibbon, M. Pilu, and R. B. Fisher, "Direct least square fitting of ellipses," *IEEE Transactions on Pattern Analysis and Machine Intelligence*, vol. 21, no. 5, pp. 476–480, 1999.